Autotaxin-mediated lipid signaling intersects with LIF and BMP signaling to promote the naive pluripotency transcription factor program

Cody Kime[a,1], Masayo Sakaki-Yumoto[b], Leeanne Goodrich[c], Yohei Hayashi[a], Salma Sami[a], Rik Derynck[b], Michio Asahi[d], Barbara Panning[c], Shinya Yamanaka[a,e,2], and Kiichiro Tomoda[a,d,2]

[a]Gladstone Institute of Cardiovascular Disease, San Francisco, CA 94158; [b]Eli and Edythe Broad Center of Regeneration Medicine and Stem Cell Research, Programs in Cell Biology and Developmental and Stem Cell Biology, Department of Cell and Tissue Biology, University of California, San Francisco, CA 94143; [c]Department of Biochemistry and Biophysics, University of California, San Francisco, CA 94158; [d]Department of Pharmacology, Faculty of Medicine, Osaka Medical College, Osaka 569-8686, Japan; and [e]Center for iPS Cell Research and Application, Kyoto University, Kyoto 606-8507, Japan

Contributed by Shinya Yamanaka, September 8, 2016 (sent for review May 27, 2016; reviewed by Paul J. Tesar and Marius Wernig)

Developmental signaling molecules are used for cell fate determination, and understanding how their combinatorial effects produce the variety of cell types in multicellular organisms is a key problem in biology. Here, we demonstrate that the combination of leukemia inhibitory factor (LIF), bone morphogenetic protein 4 (BMP4), lysophosphatidic acid (LPA), and ascorbic acid (AA) efficiently converts mouse primed pluripotent stem cells (PSCs) into naive PSCs. Signaling by the lipid LPA through its receptor LPAR1 and downstream effector Rho-associated protein kinase (ROCK) cooperated with LIF signaling to promote this conversion. BMP4, which also stimulates conversion to naive pluripotency, bypassed the need for exogenous LPA by increasing the activity of the extracellular LPA-producing enzyme autotaxin (ATX). We found that LIF and LPA-LPAR1 signaling affect the abundance of signal transducer and activator of transcription 3 (STAT3), which induces a previously unappreciated Kruppel-like factor (KLF)2-KLF4-PR domain 14 (PRDM14) transcription factor circuit key to establish naive pluripotency. AA also affects this transcription factor circuit by controlling PRDM14 expression. Thus, our study reveals that ATX-mediated autocrine lipid signaling promotes naive pluripotency by intersecting with LIF and BMP4 signaling.

naive pluripotency | LPA lipid signaling | LIF signaling | BMP4 signaling | KLF2-KLF4-PRDM14 circuit

Developmental signaling pathways, such as the leukemia inhibitory factor (LIF) and bone morphogenetic protein (BMP) pathways are key players in the establishment or maintenance of pluripotency. More recently, lysophospholipid signaling has been implicated in pluripotency (1–3). All major developmental signaling pathways function at least in part by regulating the expression of key transcription factors. Although the pathways connecting LIF and BMP to pluripotency transcription factors have been elucidated, less is known about the downstream effects of lipid signaling in pluripotency.

Pluripotent stem cells (PSCs) occur in two different states, naive and primed, which differ in their signaling requirements. These extracellular signals can affect epigenetic features in PSCs. For example, mouse naive PSCs are maintained in medium containing LIF and can be converted into primed cells by transfer into medium containing activin A and basic fibroblast growth factor (bFGF) (4). This conversion is accompanied by genome-wide alterations in DNA methylation patterns (5). In addition, primed cells such as mouse epiblast stem cells (mEpiSCs) have one active X chromosome (Xa) and one inactive X chromosome (Xi), whereas naive cells like mouse embryonic stem cells (mESCs) have two Xas. These observations indicate that altering signaling pathways can impact epigenetic features.

Whereas the conversion of naive cells to primed cells can be efficient in some circumstances, the conversion of primed cells to naive cells is more difficult to achieve. mEpiSCs are converted to mESC-like cells only after several passages on mouse embryo fibroblast (MEF) feeders in LIF-containing medium (6). This LIF-dependent conversion can be enhanced by overexpression of transcription factors NANOG, Kruppel-like factor (KLF) 2, KLF4, and/or PR domain 14 (PRDM14), but the conversion efficiencies remain low (4, 7–9). The difficulty in converting primed cells to naive cells may reflect epigenetic barriers that inhibit conversion (10) or may indicate that the relevant signaling molecules and their interactions remain to be elucidated.

We reported that culture conditions impact X chromosome inactivation (XCI) status in human induced pluripotent stem cells (hiPSCs) (11). hiPSC lines reprogrammed and maintained on LIF-expressing SNL feeder cells (12) are predominantly XaXa, whereas hiPSC lines derived on MEF feeder cells are mainly XaXi. Early-passage XaXi hiPSCs are converted to XaXa after several divisions on SNL feeder cells. These results prompted us to hypothesize that the SNL feeders produce signaling molecules, including LIF, that promote conversion from primed to naive states.

Here, we identify cytokines, nutrients, and lipids that promote reactivation of the Xi in mEpiSCs and efficiently convert primed

Significance

Naive and primed pluripotent stem cells (PSCs) provide a potential source of cells for regenerative medicine. Although both cell types can contribute to all three germ layers, they differ in cell morphology, gene expression programs, and epigenetic modifications, such as the X chromosome inactivation status. Here, we report that lysophosphatidic acid (LPA) lipid signaling and the LPA-producing enzyme autotaxin are crucial in converting primed PSCs into naive PSCs. Our results reveal relationships between signaling pathways by cytokines and the lipids that, in conjunction with nutrients, synergistically induce a transcription factor circuit necessary for establishing naive pluripotency. Thus, our study provides insights into the extracellular stimuli and gene regulation to precisely control PSCs for regenerative medicine and cell biology.

Author contributions: K.T. designed research; C.K., M.S.-Y., L.G., Y.H., S.S., and K.T. performed research; C.K., M.S.-Y., M.A., B.P., and K.T. contributed new reagents/analytic tools; C.K. and K.T. analyzed data; C.K., R.D., B.P., S.Y., and K.T. wrote the paper; and R.D., B.P., and S.Y. provided supervision.

Reviewers: P.J.T., Case Western Reserve University; and M.W., Stanford University.

Conflict of interest statement: S.Y. is a scientific advisor of iPS Academia Japan without salary. K.T. and C.K. are filing a patent related to this study.

Freely available online through the PNAS open access option.

[1]Present address: Laboratory for Retinal Regeneration, RIKEN Center for Developmental Biology, Kobe 650-0047, Japan, and Graduate School of Medicine, Kyoto University, Kyoto 606-8507, Japan.

[2]To whom correspondence may be addressed. Email: yamanaka@cira.kyoto-u.ac.jp or kiichiro.tomoda@gladstone.ucsf.edu.

This article contains supporting information online at www.pnas.org/lookup/suppl/doi:10.1073/pnas.1608564113/-/DCSupplemental.

PSCs to naive PSCs. We characterize lipid signaling in conversion to naive pluripotency, identifying the relevant receptor and downstream effector. In addition, we find that autocrine lipid production is stimulated by BMP4, indicating cross-talk between lipid signaling and BMP pathways. Finally, we show that lipid and LIF signaling both impact signal transducer and activator of transcription 3 (STAT3), which, in turn, regulates the KLF2-KLF4-PRDM14 circuit. These findings reveal the complex connections between developmental signaling pathways and transcription factors that underlie establishment and maintenance of naive pluripotency.

Results

During somatic cell reprogramming, the human Xi is reliably reactivated in hiPSCs reprogrammed on SNL feeder cells (11), implicating the LIF signaling pathway in this transition. However, LIF alone is insufficient to mediate Xi reactivation, suggesting that the SNL feeder culture condition contains additional factors that mediate this epigenetic change. To identify these factors, we used an Xi-reactivation assay that uses a primed mEpiSC reporter line. The female mEpiSC reporter line harbors a silent green fluorescent protein (GFP) transgene on the Xi (Xi-GFP), such that GFP is only expressed when the Xi is reactivated (6, 7).

Xi-GFP mEpiSCs remained GFP-negative when cultured under the feeder-free mEpiSC conditions, basal N2B27 medium containing activin A and bFGF (4) (Fig. 1 *A* and *B*). Extended culture in serum replacement-containing medium that was conditioned by SNL feeder cells (SNL-CM) activated GFP expression (GFP^+) in 6.4% of the cells (Fig. 1 *A* and *B*). This GFP^+ cell population also expressed CD31/PECAM, a marker of mouse naive PSCs (13) (Fig. 1*B*). In contrast, serum replacement-containing medium conditioned by MEFs (MEF-CM), which do not express LIF, gave rise to few GFP^+ cells (Fig. 1*B*). Furthermore, when basal N2B27 medium was supplemented with LIF and chemical inhibitors of mitogen-activated protein kinase kinase (MAPKK) and glycogen synthase kinase 3 (GSK3) (2i), which robustly sustains naive pluripotency ex vivo, only 0.3% of the cells expressed GFP (Fig. 1*B*). These results suggested that SNL-CM contains a unique activity that cooperates with LIF to efficiently promote CD31 expression and reactivate the Xi-linked GFP in mEpiSCs.

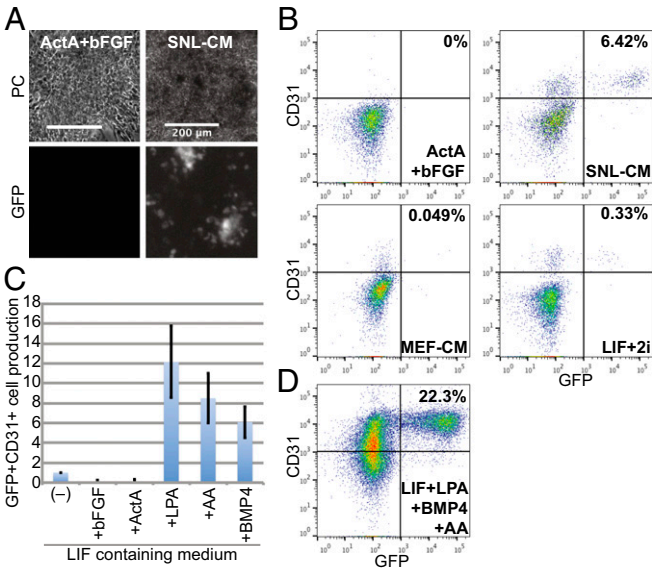

Fig. 1. Conversion medium containing LPA efficiently converts Xi-GFP mEpiSCs to GFP^+CD31^+ cells. (*A*) Cell morphology, shown using phase contrast (PC) microscopy (*Upper*), and GFP expression (*Lower*) of Xi-GFP mEpiSCs in different culture conditions. Xi-GFP mEpiSCs maintained in N2B27 medium containing activin A and bFGF (ActA+bFGF; *Left*) were GFP-negative (XaXi). After transfer to SNL-conditioned medium (SNL-CM; *Right*), some Xi-GFP mEpiSCs expressed GFP after 8 d. (Scale bars: 200 μm.) (*B*) FACS dot plots showing GFP (*x* axis) and CD31 (*y* axis) expression by cells in *A*, MEF-CM, and medium containing LIF+2i. The percentage of GFP^+CD31^+ cells is indicated in each image (upper right). $n > 5$ biological replicates. (*C*) Fold change in percentage of GFP^+CD31^+ cell generation after 13 d in N2B27 medium, supplemented with LIF and the indicated factors relative to LIF alone. Mean ± SD, $n = 3$ biological replicates. (*D*) FACS dot plots showing GFP (*x* axis) and CD31 (*y* axis) expression in N2B27 medium, supplemented with LIF, BMP4, AA, and LPA (conversion medium) at day 8 of conversion. $n > 5$ biological replicates.

To identify factors that promote conversion into GFP^+CD31^+ cells, we tested whether bioactive molecules found in SNL-CM and MEF-CM affected Xi reactivation in mEpiSCs. Both media contain lysophosphatidic acid (LPA), ascorbic acid (AA), bFGF, and a BMP-like activity (14), whereas LIF is present only in SNL-CM, and activin A is enriched in MEF-CM (Fig. S1*A*). We evaluated the individual effects of these bioactive molecules on the generation of GFP^+CD31^+ cells from Xi-GFP mEpiSCs by adding each of them to basal N2B27 medium supplemented with LIF. BMP4 was used to provide the BMP-like activity as it has been implicated in conversion to naive pluripotency (15). Addition of bFGF or activin A suppressed the generation of GFP^+CD31^+ cells relative to LIF alone, whereas addition of LPA, AA, or BMP4 increased their relative proportion (Fig. 1*C*). These results suggest that bFGF and activin A suppress the transition to naive pluripotency, which may explain why MEF-CM does not support the production of GFP^+CD31^+ cells despite the presence of the stimulatory factors LPA, AA, and the BMP-like activity.

Treatment with basal N2B27 medium supplemented with LIF, LPA, BMP4, and AA (conversion medium) resulted in the conversion of 22.3% of the Xi-GFP mEpiSCs into GFP^+CD31^+ cells, a substantially higher percentage than the 6.4% conversion seen with SNL-CM (Fig. 1*D* and Fig. S1 *B* and *C* using different mEpiSC lines). The GFP^+CD31^+ cells exhibited the hallmarks of naive pluripotency, including Xi-reactivation and germ-line transmission (Figs. S1 *D* and *E* and S2 *A*–*F*). These results identify LIF, LPA, BMP4, and AA as key signaling molecules that cooperate to convert primed PSCs into naive PSCs.

Lipid signaling is emerging as a player in establishment and maintenance of pluripotency (1–3). To determine whether there are specific lipid requirements in the conversion to naive pluripotency, we assayed the effects of replacing LPA with other lipids in a minimal conversion system that employs only LIF and lipids. LIF and LPA promoted the generation of GFP^+CD31^+ cells more efficiently than LIF or LPA alone (Fig. 2 *A* and *B*), demonstrating synergy between LIF and LPA. Another lysophospholipid (LP), sphingosine-1-phosphate, also cooperated with LIF in the generation of GFP^+CD31^+ cells, albeit much less efficiently than LPA (Fig. 2*B*). In contrast, a mixture of chemically defined lipids containing cholesterol and several types of fatty acids, but no LPs, did not increase the yield of LIF-induced GFP^+CD31^+ cells (Fig. 2*B*). Therefore, LPs, and not all fatty acids, are the signaling molecules relevant for production of GFP^+CD31^+ cells.

Endogenous LPA from cultured cells is produced by the secreted enzyme autotaxin (ATX) (16–18). ATX catalyzes the generation of LPA from lysophosphatidylcholine, which is released from apoptotic cells (19) (Fig. 3*A*). During our conversion experiments, we found that ATX mRNA was expressed in mEpiSCs. Additionally, we could detect ATX in mEpiSC culture supernatant (conditioned media), indicating that these PSCs secrete ATX. To determine whether ATX is active in conditioned media, we quantitatively measured ATX enzymatic activity using a fluorogenic ATX substrate and found conditioned media exhibited increased activity relative to unconditioned media (Fig. 3*B*). We then examined whether ATX affects reactivation of the Xi by chemically inhibiting it with HA-130 (20). Addition of HA-130 to conversion medium did not affect production of GFP^+ cells (+ATXi). However, addition of HA-130 to the conversion medium lacking LPA

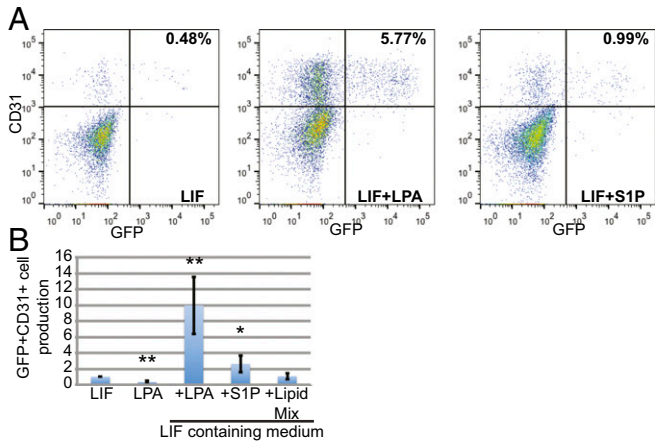

Fig. 2. Lysophospholipids, especially LPA, collaborate with LIF in GFP$^+$CD31$^+$ cell production. (*A*) FACS dot plots showing GFP (*x* axis) and CD31 (*y* axis) expression following culture of Xi-GFP mEpiSCs in media containing LIF alone, LIF+LPA, or LIF+S1P for 13 d. (*B*) Conversion efficiency of Xi-GFP mEpiSCs in indicated culture conditions relative to LIF alone. $n = 3$ for LIF+Lipid Mix and $n = 4$ for other conditions. Mean ± SD. Two-tailed unpaired *t* test. *$P < 0.05$ and **$P < 0.01$ vs. LIF alone.

(–LPA+ATXi) resulted in a substantial reduction in the generation of GFP$^+$ cells (Fig. 3*C*) relative to ATX inhibition or removal of LPA individually. These results suggest that endogenous LPA production contributes to the reactivation of the Xi.

We next asked whether BMP4 or AA affects ATX activity to determine whether there is cross-talk between these signaling molecules. Xi-GFP mEpiSCs were treated with LIF+AA, LIF+BMP4, or LIF+BMP4+AA, and the ATX activity in the media was determined (Fig. 3*D*). Media containing LIF+BMP4 exhibited increased ATX activity compared with media containing LIF+AA. LIF+BMP4+AA containing media exhibited comparable ATX activity to LIF+BMP4 media, suggesting that BMP4, and not AA, regulates ATX activity. ATX activity did not correlate directly with the GFP$^+$ cell number (Fig. 3*E*), as LIF+BMP4+AA medium (–LPA medium) produced more GFP$^+$ cells than LIF+BMP4 medium (–LPA-AA medium) despite showing comparable ATX activity. Furthermore, the amount of secreted ATX was not obviously different between LIF+AA and LIF+BMP4 treatment (Fig. 3*F*), suggesting that BMP4 signaling increases ATX activity without affecting protein abundance.

To determine the contribution of each factor to Xi-GFP reactivation, we assessed the effects of removing each component of the conversion media on production of GFP$^+$ cells. Removing LPA from conversion medium did not result in a substantial loss of GFP$^+$ cells, removing LIF largely eliminated production of GFP$^+$ cells, and removing AA or BMP4 resulted in partial loss of GFP$^+$ cells (Fig. 3*E*). Because LPA removal did not have a dramatic effect, there is the potential for redundancy with BMP4 or AA. Therefore, we examined the effects of removing both LPA and AA or LPA and BMP4. When both LPA and AA were removed, there was no significant reduction in GFP$^+$ cells relative to removing AA alone. In contrast, when both LPA and BMP4 were removed, there was a greater reduction than removing BMP4 alone. These results suggest that LPA signaling functions independently of AA activity and are consistent with the possibility that BMP4 enhancement of endogenous ATX activity generates a sufficient amount of endogenous LPA for efficient Xi reactivation.

The role for LPA in promoting efficient conversion of primed PSCs into naive PSCs raised the question of what signaling pathway might be involved. LPA binds to and acts through a family of six G protein-coupled LPA receptors (LPARs) to initiate signaling in target cells (16). We therefore examined whether LPA-LPAR signaling is involved in conversion to naive pluripotency. Ki16425, a competitive inhibitor of LPAR1 and LPAR3 (16) significantly reduced the generation of GFP$^+$CD31$^+$ cells in response to LIF+LPA (Fig. 4*A*). Additionally, shRNA-mediated depletion of LPAR1, but not LPAR3, substantially decreased the generation of GFP$^+$ cells produced by conversion medium (Fig. 4*B*). These results suggest that LPA-induced activation of LPAR1 promotes Xi reactivation and that signaling through LPAR1 and LPAR3 may play a role in conversion to naive pluripotency.

LPAR activation induces diverse signaling events via PKA, PKC, MAPKK, GSK3β, PI3K, and Rho-associated protein kinase (ROCK) (16). Additionally, LPA directly activates peroxisome proliferator-activated receptor-γ independent of LPAR (16). Using selective chemical inhibitors, activators, and modulators, we queried the pathways activated by LPA to promote the generation of GFP$^+$CD31$^+$ cells (Fig. S3*A*). Among the small molecules tested, the highly selective ROCK inhibitor Y-27632 (21) and the less-selective ROCK inhibitor Thiazovivin (22) each reduced the production of GFP$^+$CD31$^+$ cells induced by LIF and LPA

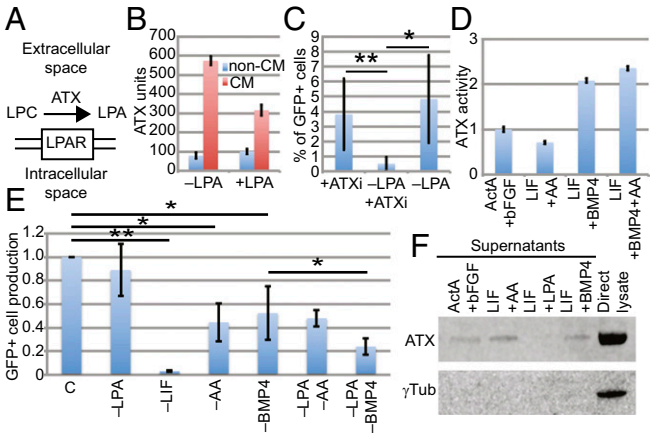

Fig. 3. The LPA-producing enzyme ATX induced by BMP4 signaling promotes the Xi reactivation. (*A*) Diagram showing cells secreting ATX that catalyzes the production of LPA from extracellular lysophosphatidylcholine (LPC). (*B*) ATX enzymatic activity in medium without or with added LPA, as shown. Media conditioned with Xi-GFP mEpiSCs were collected at day 6 of conversion (red). The same media, which were not conditioned with cells (blue), served as controls (blue). Addition of LPA resulted in decreased ATX activity, consistent with the reducing ATX activity in vitro with high concentrations of LPA (31) or deceasing ATX protein in an LPA containing medium shown in *F*. Mean ± SD of technical duplicates. The data represent one of three independent experiments. (*C*) Percentage of GFP$^+$ cells after 6 d of Xi-GFP mEpiSC culture in conversion medium supplemented with HA-130 (+ATXi), or supplemented with HA-130 and lacking LPA (–LPA+ATXi), or lacking LPA (–LPA). Mean ± SD of biological replicates. $n = 4$ for –LPA, $n = 5$ for +ATXi, and –LPA+ATXi. Two-tailed unpaired *t* tests. *$P < 0.05$ and **$P < 0.01$. (*D*) Fold change in ATX activity in media supplemented with indicated factors and conditioned with cells at day 6 of conversion experiments. The ATX activity in medium supplemented with activin A and bFGF is set as 1.0. Mean ± SD of technical duplicates. The data represent one of three independent experiments. (*E*) Relative efficiency of generation of GFP$^+$ cells from Xi-GFP mEpiSCs in different media. The percentage of GFP$^+$ cells in conversion medium is set as 1.0. Mean ± SD of biological replicates at day 6. $n = 8$ for conversion medium (C), $n = 7$ for conversion medium lacking LPA (–LPA), $n = 6$ for conversion medium lacking AA (–AA) or lacking BMP4 (–BMP4), $n = 3$ for conversion medium lacking LPA and AA (–LPA–AA), lacking LPA and BMP4 (–LPA–BMP4), or lacking LIF (–LIF). Two-tailed unpaired *t* test. *$P < 0.05$ and **$P < 0.01$. (*F*) Western blots showing expression levels of ATX and γTub in cell culture supernatants during conversion. γTub is not detected in the cell culture supernatants, suggesting ATX in the supernatants are secreted from the cells. Addition of LPA in a medium decreases ATX proteins, consistent with decreasing ATX activity shown in *B*. In contrast, addition of BMP4 in a medium does not obviously affect ATX protein level despite increasing ATX activities shown in *D*.

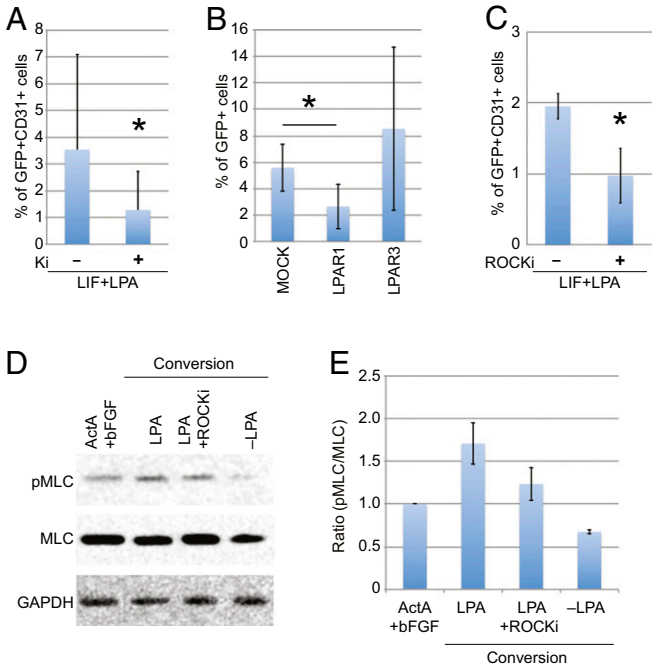

Fig. 4. LPA-LPAR-ROCK signaling promotes GFP$^+$CD31$^+$ cell production. (*A*) Conversion efficiency of Xi-GFP mEpiSCs, expressed as percentage of GFP$^+$CD31$^+$ cells generated in different conditions for 13 d. Ki16425 (Ki) is a competitive inhibitor for LPAR1 and LPAR3. Mean + SD of biological replicates. n = 23 for LIF+LPA, and n = 5 for LIF+LPA+Ki. Two-tailed unpaired t test. *P < 0.05. (*B*) Percentage of GFP$^+$ cells cultured in conversion medium for 6 d after silencing LPAR1 or LPAR3 expression using shRNA. Mean ± SD of biological replicates. n = 5 for MOCK control, and n = 4 for LPAR1 and LPAR3. Two-tailed unpaired t test. *P < 0.05. (*C*) Conversion efficiency of Xi-GFP mEpiSCs, expressed as percentage of GFP$^+$CD31$^+$ cells when Xi-GFP mEpiSCs were cultured in LIF+LPA medium with or without the ROCK inhibitor Y-27632 for 13 d. Mean ± SD n = 3, biological replicates, two-tailed unpaired t test. *P < 0.05. (*D*) Western blots showing expression levels of phosphorylated and unphosphorylated MLC (pMLC and MLC, respectively), and glyceraldehyde-3-phosphate dehydrogenase (GAPDH) in Xi-GFP mEpiSCs cultured in mEpiSC medium (ActA+bFGF), conversion medium (LPA), conversion medium supplemented with ROCK inhibitor (LPA+ROCKi), or conversion medium lacking LPA (–LPA) for 7 d. The Western blots represent one of two sets of independent experiments. (*E*) Ratio of pMLC over MLC expression. Band intensities for pMLC and MLC were quantified after Western blotting as shown in *D*, and the ratios were calculated. Fold changes in the ratios relative to those in mEpiSC medium (ActA+bFGF) are shown. Mean ± SD, n = 2 biological replicates.

(Fig. 4*C* and Fig. S3*B*), suggesting a role for ROCK in the conversion to naive pluripotency. To determine whether LPA signals through ROCK during conversion, we examined the effects of LPA treatment on the phosphorylation of myosin light chain (MLC), a direct target of ROCK phosphorylation (23). We found that MLC exhibited increased phosphorylation in Xi-GFP mEpiSCs treated with conversion medium containing LPA relative to conversion medium without LPA. The increased MLC phosphorylation was attenuated by ROCK inhibition (Fig. 4 *D* and *E*). These results suggest that LPA-induced ROCK activation plays a key role in the conversion from primed to naive pluripotency. Because ROCK signaling lies downstream of LPAR1 and not LPAR3 (16), these results, together with our LPAR1 and LPAR3 knockdown results, suggest that LPAR1 is likely to be the key receptor for LPA signaling during conversion.

To determine how LPA signaling is involved in establishing naive pluripotency, we examined its role in induction of the transcription factors KLF2, KLF4, and PRDM14. Overexpression of these transcription factors in mEpiSCs promotes naive pluripotency (4, 7). We determined levels of KLF2, KLF4, PRDM14, and NANOG RNA at 24-h intervals after transferring Xi-GFP mEpiSCs to conversion medium. KLF2, KLF4, and PRDM14 exhibited different kinetics of up-regulation (Fig. 5*A*). KLF2 and KLF4 reached nearly maximal levels at day 2 (Fig. 5*A*). PRDM14 was not induced until day 2–3 and reached maximal levels at day 4 (Fig. 5*A*). In contrast, NANOG was highly expressed in Xi-GFP mEpiSCs, and its levels were transiently reduced at day 2 of treatment with conversion medium (Fig. 5*A*). These findings indicate that conversion medium robustly induces KLF2, KLF4, and PRDM14 expression. Since GFP$^+$CD31$^+$ cells emerged after day 5 (Fig. 5*B*), the transcription factors associated with naive pluripotency and required for efficient conversion (Fig. 5*C*) were expressed before GFP$^+$CD31$^+$ cells appeared.

To assess the contribution of each component of conversion medium on regulation of naive pluripotency transcription factors, we tested the effects of conversion medium lacking LPA (–LPA), BMP4 (–BMP4), AA (–AA), or LIF (–LIF) on expression of KLF2, KLF4, PRDM14, and NANOG. In the –LPA medium, transcription factor expression did not change significantly relative to conversion medium (Fig. 5*D*), consistent with our finding that BMP4 stimulates production of LPA by regulating ATX activity. In contrast, when we individually removed BMP4, AA, or LIF from the conversion medium, we observed decreased expression of these transcription factors (Fig. 5*D*). In the –LIF medium, PRDM14 and KLF2 induction were substantially reduced (Fig. 5*D*). Removing BMP4 or AA had different effects on transcription factor expression (Fig. 5*D*). PRDM14 expression was reduced under both conditions. NANOG expression decreased more in –AA, whereas KLF4 expression decreased more in –BMP4 (Fig. 5*D*). Thus, LIF, BMP4, and AA have differing effects on expression of pluripotency transcription factors.

Removing LPA from the conversion medium did not show substantial effects on GFP$^+$ cell production (Fig. 3*E*) and induction

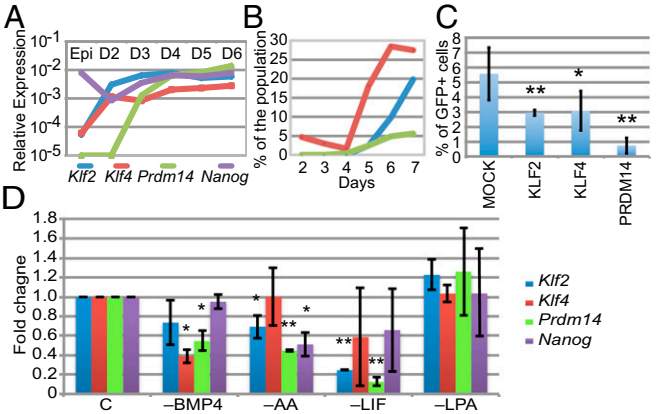

Fig. 5. Conversion medium induces transcription factors associated with naive pluripotency. (*A*) Expression levels of the transcription factors *Klf2*, *Klf4*, *Prdm14*, and *Nanog* during conversion. The expression levels shown are relative to expression levels of *Gapdh* in parental Xi-GFP mEpiSCs (far left lane) or at the indicated times (day 2 to day 6). The chart represents one of two sets of independent experiments. (*B*) Percentage of GFP$^+$CD31$^+$ (blue), CD31$^+$ (red), and GFP$^+$ (green) cells during the conversion (day 2 to day 7) determined by FACS. The chart represents one of two sets of independent experiments. (*C*) Percentage of GFP$^+$ cells cultured in conversion medium for 6 d after knockdown of targets indicated (x axis). n = 5 for MOCK control and n = 4 for other conditions. Mean ± SD. Two-tailed unpaired t test. *P < 0.05, **P < 0.01 vs. MOCK. (*D*) Fold change in the expression of the transcription factors *Klf2*, *Klf4*, *Prdm14*, and *Nanog*, cultured in conversion medium, or conversion medium lacking BMP4 (–BMP4), AA (–AA), LF (–LIF), or LPA (–LPA). Values are relative to those in conversion medium. n = 4 biological replicates. Mean ± SD. Two-tailed unpaired t test. *P < 0.05, **P < 0.01 vs. conversion.

of key transcription factors (Fig. 5*D*). However, because the inhibition of LPA-LPAR1 signaling significantly impaired the conversion of primed cells to GFP^+CD31^+ cells (Fig. 4 *A* and *B*), we examined effects of the depletion of LPAR1 on the expression of pluripotency transcription factors in conversion medium. In LPAR1-depleted cells, the transcription factors, KLF2, KLF4, and NANOG, were decreased relative to those in control cells (Fig. 6*A*). These results suggest that LPA-LPAR1 signaling affects establishment of the naive pluripotency gene expression pattern.

LIF signaling modulates activity of the transcription factor STAT3, prompting us to ask whether the LPA and LIF pathways intersect via STAT3. We examined whether LPAR1 signaling affects STAT3 by comparing the effects of LPAR1 depletion with those of depleting STAT3, KLF2, KLF4, or PRDM14. In addition to decreasing expression of KLF2, KLF4, and PRDM14, LPAR1 and STAT3 knockdown each decreased expression of suppressor of cytokine signaling 3 (SOCS3), a direct target of LIF-STAT3 signaling (Fig. 6*A*). LPAR1 likely acts upstream of STAT3, because LPAR1 depletion decreased expression of STAT3. These results suggest that LPAR1 signaling intersects the LIF-STAT3 pathway in the regulation of these naive pluripotency transcription factors. Additionally, because LPAR1 depletion, and not STAT3 depletion, decreased NANOG expression, LPAR1 signaling may regulate NANOG independent of LIF-STAT3 signaling. Knockdown of KLF2, KLF4, or PRDM14 resulted in similar changes, with depletion of each factor significantly decreasing expression of the others without affecting STAT3 or SOCS3 (Fig. 6*A*). Taken together, these results suggest that LIF and LPA signaling pathways synergistically induce or maintain the KLF2-KLF4-PRDM14 transcription factor circuit to reactivate the Xi and establish naive pluripotency (Fig. 6*B*).

Discussion

In this study, we identify activities that promote (LIF, LPA, AA, and BMP4) and antagonize (activin A and bFGF) conversion of mouse primed to naive PSCs. Combining LIF, BMP4, AA, and LPA and omitting activin A and bFGF, substantially promoted formation of naive PSCs. These results build on the growing body of work that indicates that pluripotent cell identity is shaped by a combination of signaling proteins and bioactive compounds. Our results also indicate that using the correct combination of bioactive molecules and developmental signals is sufficient to efficiently convert primed PSCs to naive PSCs.

Regulation of Key Transcription Factors. LIF, AA, and BMP4 individually or synergistically induced and maintained the key transcription factors KLF2, KLF4, PRDM14, and NANOG. Depletion of KLF2, KLF4, and PRDM14 inhibited conversion to naive pluripotency. Together these findings suggest that induction of naive pluripotency transcription factors in primed cells by these signaling molecules forms a transcription factor circuit that drives the conversion to the naive state.

Our data indicate that LPA-LPAR1 and LIF control STAT3, which, in turn, regulates KLF2, KLF4, and PRDM14. Thereafter, KLF2, KLF4, and PRDM14 regulate each other and form a transcription factor circuit, because depletion of any one affected the expression of the others. KLF2 and KLF4 were up-regulated before PRDM14, suggesting that the LIF/AA/BMP4-mediated increase in KLF2 and KLF4 expression promotes PRDM14 expression and sets up the circuit. AA may affect epigenetic status of the loci encoding these transcription factors by modulating the activity of TET DNA hydroxymethylase family proteins and histone demethylases (24, 25).

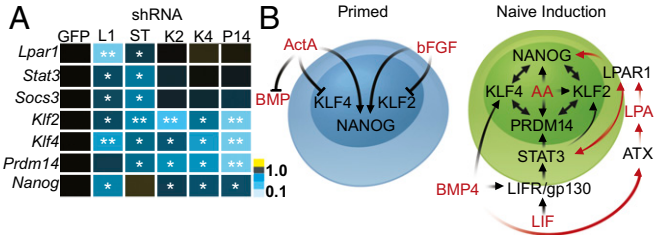

Fig. 6. LPAR1 signaling intersects with STAT3 and NANOG during conversion. (*A*) Heat map showing relative expression levels of the genes (left) analyzed in shRNA-expressing cells (top) examined after 6 d of culture in conversion medium. The expression levels in GFP shRNA-expressing cells are set as 1. The expression level color indicator is shown on the right. $n = 3$ biological replicates. Two-tailed unpaired *t* test. $^*P < 0.05$, $^{**}P < 0.01$ vs. GFP. L1, LPAR1; ST, STAT3; K2, KLF2; K4, KLF4; P14, PRDM14. (*B*) Model showing relationships among the cytokines, nutrients, and lipids, and transcription factors in establishing naive pluripotency. Arrows indicate direct and indirect relationships. Red arrows indicate connection among BMP4, ATX, LPAR1, STAT3 and NANOG revealed in this study.

Lipid Signaling Pathways in Conversion. LPA and lipid signaling pathways are emerging as important players in maintaining pluripotency in mouse and human PSCs (1–3, 26, 27). Our inhibitor and knockdown studies identify downstream signaling components and reveal a connection with naive pluripotency transcription factors. Our data indicate that the LPA receptor LPAR1 acts through ROCKs to promote conversion to naive pluripotency. ROCKs regulate many processes, but they are best known for control of cytoskeletal organization and cell-cell junctions. Identification of the ROCK targets that are important for conversion has the potential to provide insight into how changes in cellular architecture may be coordinated with changes in gene expression.

Interplay Among LPA, LIF, and LPA Signaling in Promoting Naive Pluripotency. Our data suggest that LPA-LPAR1 signaling impacts naive pluripotency by modulating expression of STAT3. This result suggests LIF and LPA-LPAR1 signaling have a common target. Understanding whether LPA-LPAR1 controls STAT3 via the same kinases that lie downstream of LIF, or whether a different type of regulation is used, will be central to elucidate the wiring diagram underlying naive pluripotency.

We show that BMP4 stimulates the activity of the LPA producing enzyme ATX. Thus, ATX is a nexus of LPA and BMP4 signaling. Our results suggest that BMP4 impacts pluripotency by affecting endogenous lipid signaling in addition to or as a result of its better-known roles in SMAD regulation and stimulating the production of LIF receptor (15). Because the amount of secreted ATX was not changed by BMP4 addition, BMP4 signaling may regulate ATX activity at the level of posttranslational modification or cofactor abundance. Up-regulation of ATX in several types of cancers is correlated with invasiveness and metastatic potential (28). Our findings connecting ATX activity and developmental signaling pathways, which are also dysregulated in many cancers, may provide a useful avenue to dissect activities that promote these devastating diseases.

Our results suggest two key signaling pathways, LIF and BMP4 signaling, are connected with ATX-mediated autocrine LPA signaling in regulation of PSCs. The intersection of LPA signaling with both BMP4 and LIF signaling reveals further complexity in the pathways used to establish or maintain naive pluripotency.

ATX is expressed in mESCs and in early embryos, consistent with a role for autocrine LPA signaling in development. Whereas exogenous LPA may support naive pluripotency ex vivo, the embryo may rely on the LPA precursor lysophosphatidylcholine, which is released as a part of microvesicles that are shed from uterine cells (29, 30). Therefore, scavenging autocrine lipid signaling mediated by ATX may play a role in promoting naive pluripotency in culture and in vivo.

Implication in Human PSCs. Most human PSCs (hPSCs) more closely resemble mEpiSCs than mESCs in growth properties, gene expression, and epigenetic features, suggesting that hPSCs may be in

the primed state. Recently, many methods to convert hPSCs into mESC-like cells have been reported. In one instance, a medium containing LPA combined with kinase inhibitors and growth on feeder cells converted hPSCs to naive-like cells (3). Consistent with a potential role for LPA signaling in human pluripotency regulation, hPSCs express ATX, LPARs, and their downstream effectors. These observations raise the possibility that a combination of lipids, cytokines, and nutrients may also promote human naive pluripotency. Generation of naive hPSCs with chemically defined media that employs nutrients and developmental signaling molecules, and not exogenous gene expression or inhibitors with unknown side effects, may be beneficial for regenerative medicine.

Materials and Methods

Cell Culture. Xi-GFP mEpiSCs were kindly provided by Azim Surani and Siqin Bao, The Gurdon Institute, Cambridge, UK, and were routinely maintained on plates coated with fibronectin (Sigma) (feeder-free condition) in N2B27 basal medium (Ndiff 227 medium; from StemCells and later from Clontech) supplemented with 20 ng/mL activin A (R&D Systems) and 12 ng/mL bFGF (Millipore). Cells were passaged every 2–3 d at a 1:20 dilution from a previous culture after detachment/scraping and dissociation with Accutase (Millipore). Another mEpiSC line (PT, RB, and RB Yellow lines) was kindly provided by Paul Tesar, Case Western Reserve University, Cleveland, and Robert Blelloch, University of California, San Francisco, and were maintained in the same way as Xi-GFP mEpiSCs.

Blastocyst Injection and F_1 Mouse Production. Single GFP^+CD31^+ cells or mKate-expressing Xi-GFP mEpiSCs were injected into blastocysts from C57BL/6 mice. GFP or mKate fluorescence was used to assess chimerism at embryonic day (E) 14.5, and coat color was used to assess chimerism in pups. Highly chimeric F_0 female mice were crossed with C57BL/6 male mice to obtain F_1 offspring. These protocols were approved by the Institutional Animal Care and Use Committee at University of California, San Francisco.

Conversion Experiments. Single-cell suspensions of Xi-GFP mEpiSCs were made with Accutase, and the single cells were seeded on fibronectin-coated six-well plates in medium containing activin A and bFGF 1 d before starting conversion experiments. At 24 h after seeding, the medium was replenished with fresh medium (negative control) or changed to an assay medium indicated at each experiment to start the conversion. The assay medium was changed every 24 h, and GFP fluorescence was checked daily by microscopic inspection for 6 and 8 (with 20,000 starting cells) to 13 d (with 3,000 starting cells). The assay media contained 1,000 units LIF (Millipore), 1–10 ng/mL BMP4 (R&D Systems), 64 μg/mL L-ascorbic acid 2-phosphate (Sigma), 10–100 nM LPA (Avanti Polar Lipids), and/or 0.1–1 μM OMPT (Avanti Polar Lipids) in N2B27 basal medium (StemCells, now Clontech) for use in Figs. 1 *A*–*C*, 3 *A* and *B*, and 4 *A* and *C*, or prepared by ourselves for use in other conversion experiments. The in-house N2B27 medium consists of DMEM/F12+GlutaMax (500 mL), Neurobasal medium (500 mL), N2 supplement (5 mL), B27 supplement (10 mL), 7.5% (vol/vol) BSA fraction V (666 μL), and GlutaMax (5 mL/L) (all from Life Technologies). To narrow down signaling pathways that are involved in conversion, the chemical inhibitors, activators, and modulators were used at concentrations as indicated below: 10 ng/mL mouse WNT3a (R&D Systems), 3 μM CHIR99021 (Stemgent), Forskolin (Sigma), 0.1 and 0.01 mM IBMX (Sigma), 1 μM GW1929 (Selleckchem), 1 μM SR1664 (Selleckchem), 1 μM Y27632 (Sigma), and 1 μM Thiazovivn (Selleckchem). Conversion efficiencies were determined by counting GFP-positive cell clusters or by flow cytometry. To select converted cells, cells were cultured in conversion medium for 6–9 d, passaged, and cultured on plates coated with laminin 511 or iMatrix (Nippi/Iwai North America) in 50:50 of conversion medium:LIF+2i medium [N2B27 medium supplemented with 1,000 units LIF (Millipore), 1 μM PD0325901 (Selleckchem), and 3 μM CHIR99021 (Stemgent)]. The next day, the medium was changed to LIF+2i medium. A nearly pure converted cell population was obtained within a few passages. There was not massive cell death upon transition to 2i+LIF, suggesting that even cells that were not $CD31^+$ after treatment with conversion medium converted upon culture in 2i+LIF.

ACKNOWLEDGMENTS. We thank Drs. Siquin Bao and Azim Surani for kindly providing Xi-GFP mEpiSCs; Drs. Paul Tesar and Robert Blelloch for other mEpiSC lines; Dr. Mohammad Mandegar for the U6-BsmBI-CNKB vector; members of S.Y. laboratory for useful discussions; and our Stem Cell Core, Flow Cytometry Core and Transgenic Core, Kazuto Suzuki, Yoshimune Takagi, Marcia Mednick, Gary Howard, Crystal Herron, Karena Essex, Moe Fukuzaki, Sayaka Takeshima, Yoko Miyake, and members of the M.A. laboratory for their support. Dr. Masayo Takahashi provided financial support, B.P. is funded by NIH Grant R01 GM088506, and this work was also supported by funding from Kyoto University grants and the Gladstone Institutes; L.K. Whittier Foundation and the Roddenberry Foundation; National Heart, Lung, and Blood Institute/NIH Grants U01-HL100406 and U01-HL098179; the University of California San Francisco-Gladstone Institute of Virology & Immunology Center for AIDS Research, an NIH-funded program from Grant P30 AI027763 and instrument grant NIH S10 RR028962-01; and from the California Institute for Regenerative Medicine (CIRM). The Gladstone Institutes received support from a National Center for Research Resources Grant RR18928-01. K.T. was a scholar of the CIRM.

1. Blauwkamp TA, Nigam S, Ardehali R, Weissman IL, Nusse R (2012) Endogenous Wnt signalling in human embryonic stem cells generates an equilibrium of distinct lineage-specified progenitors. *Nat Commun* 3:1070.
2. Garcia-Gonzalo FR, Izpisúa Belmonte JC (2008) Albumin-associated lipids regulate human embryonic stem cell self-renewal. *PLoS One* 3(1):e1384.
3. Qin H, et al. (2016) YAP induces human naive pluripotency. *Cell Reports* 14(10): 2301–2312.
4. Guo G, et al. (2009) Klf4 reverts developmentally programmed restriction of ground state pluripotency. *Development* 136(7):1063–1069.
5. Hackett JA, et al. (2013) Synergistic mechanisms of DNA demethylation during transition to ground-state pluripotency. *Stem Cell Rep* 1(6):518–531.
6. Bao S, et al. (2009) Epigenetic reversion of post-implantation epiblast to pluripotent embryonic stem cells. *Nature* 461(7268):1292–1295.
7. Gillich A, et al. (2012) Epiblast stem cell-based system reveals reprogramming synergy of germline factors. *Cell Stem Cell* 10(4):425–439.
8. Silva J, et al. (2009) Nanog is the gateway to the pluripotent ground state. *Cell* 138(4): 722–737.
9. Hayashi Y, et al. (2015) Structure-based discovery of NANOG variant with enhanced properties to promote self-renewal and reprogramming of pluripotent stem cells. *Proc Natl Acad Sci USA* 112(15):4666–4671.
10. Mansour AA, et al. (2012) The H3K27 demethylase Utx regulates somatic and germ cell epigenetic reprogramming. *Nature* 488(7411):409–413.
11. Tomoda K, et al. (2012) Derivation conditions impact X-inactivation status in female human induced pluripotent stem cells. *Cell Stem Cell* 11(1):91–99.
12. McMahon AP, Bradley A (1990) The Wnt-1 (int-1) proto-oncogene is required for development of a large region of the mouse brain. *Cell* 62(6):1073–1085.
13. Rugg-Gunn PJ, et al. (2012) Cell-surface proteomics identifies lineage-specific markers of embryo-derived stem cells. *Dev Cell* 22(4):887–901.
14. Xu RH, et al. (2005) Basic FGF and suppression of BMP signaling sustain undifferentiated proliferation of human ES cells. *Nat Methods* 2(3):185–190.
15. Onishi K, Tonge PD, Nagy A, Zandstra PW (2014) Local BMP-SMAD1 signaling increases LIF receptor-dependent STAT3 responsiveness and primed-to-naive mouse pluripotent stem cell conversion frequency. *Stem Cell Rep* 3(1):156–168.
16. Choi JW, et al. (2010) LPA receptors: Subtypes and biological actions. *Annu Rev Pharmacol Toxicol* 50:157–186.
17. Moolenaar WH, Perrakis A (2011) Insights into autotaxin: How to produce and present a lipid mediator. *Nat Rev Mol Cell Biol* 12(10):674–679.
18. Perrakis A, Moolenaar WH (2014) Autotaxin: Structure-function and signaling. *J Lipid Res* 55(6):1010–1018.
19. Lauber K, et al. (2003) Apoptotic cells induce migration of phagocytes via caspase-3-mediated release of a lipid attraction signal. *Cell* 113(6):717–730.
20. Albers HM, et al. (2010) Boronic acid-based inhibitor of autotaxin reveals rapid turnover of LPA in the circulation. *Proc Natl Acad Sci USA* 107(16):7257–7262.
21. Uehata M, et al. (1997) Calcium sensitization of smooth muscle mediated by a Rho-associated protein kinase in hypertension. *Nature* 389(6654):990–994.
22. Xu Y, et al. (2010) Revealing a core signaling regulatory mechanism for pluripotent stem cell survival and self-renewal by small molecules. *Proc Natl Acad Sci USA* 107(18):8129–8134.
23. Amano M, et al. (1996) Phosphorylation and activation of myosin by Rho-associated kinase (Rho-kinase). *J Biol Chem* 271(34):20246–20249.
24. Monfort A, Wutz A (2013) Breathing-in epigenetic change with vitamin C. *EMBO Rep* 14(4):337–346.
25. Blaschke K, et al. (2013) Vitamin C induces Tet-dependent DNA demethylation and a blastocyst-like state in ES cells. *Nature* 500(7461):222–226.
26. Todorova MG, Fuentes E, Soria B, Nadal A, Quesada I (2009) Lysophosphatidic acid induces Ca2+ mobilization and c-Myc expression in mouse embryonic stem cells via the phospholipase C pathway. *Cell Signal* 21(4):523–528.
27. Avery K, Avery S, Shepherd J, Heath PR, Moore H (2008) Sphingosine-1-phosphate mediates transcriptional regulation of key targets associated with survival, proliferation, and pluripotency in human embryonic stem cells. *Stem Cells Dev* 17(6):1195–1205.
28. Stracke ML, et al. (1992) Identification, purification, and partial sequence analysis of autotaxin, a novel motility-stimulating protein. *J Biol Chem* 267(4):2524–2529.
29. Braundmeier AG, Dayger CA, Mehrotra P, Belton RJ, Jr, Nowak RA (2012) EMMPRIN is secreted by human uterine epithelial cells in microvesicles and stimulates metalloproteinase production by human uterine fibroblast cells. *Reprod Sci* 19(12):1292–1301.
30. Ng YH, et al. (2013) Endometrial exosomes/microvesicles in the uterine microenvironment: A new paradigm for embryo-endometrial cross talk at implantation. *PLoS One* 8(3):e58502.
31. van Meeteren LA, et al. (2005) Inhibition of autotaxin by lysophosphatidic acid and sphingosine 1-phosphate. *J Biol Chem* 280(22):21155–21161.

Supporting Information

Kime et al. 10.1073/pnas.1608564113

SI Materials and Methods

Flow Cytometry. For the flow cytometric analyses, we made single-cell suspensions of Xi-GFP mEpiSCs with Accutase. The single cells were stained with a CD31 (PECAM) antibody (Clone MEC13.3/BD Bioscience) conjugated with allophycocyanin. The stained cells were analyzed with MACSQuant VYB and FlowJo software.

ELISA. The concentrations of LIF and activin A in the indicated media were determined by using ELISA. We used mouse LIF and human/mouse/rat activin A Quantikine ELISA kits (R&D Systems), according to the manufacturer's instructions.

RNA FISH. Probe preparation and FISH procedure were described (29). Briefly, the FISH probes were prepared with a Bioprime kit (Life Technologies), according to the manufacturer's instruction. Xi-GFP mEpiSCs and GFP^+CD31^+ cells were harvested with Accutase to make a single-cell suspension, and the single cells were spun on a glass slide with Cytospin (Thermo Fisher Scientific, product no. A78300003) at 800 rpm for 3 min. These samples were then permeabilized, fixed with 4% (vol/vol) paraformaldehyde for 10 min, and stored in 70% (vol/vol) EtOH at 4 °C overnight or longer. The samples were then dehydrated in 85–100% (vol/vol) EtOH and hybridized with the probes at 37 °C overnight. After hybridization, the samples were extensively washed, mounted with antifade mounting medium (Vectashield) on a slide glass, and examined by microscopy with a 100× oil lens. More than 200 cells in each sample were scored.

Serum Replacement-Containing Medium and CMs. Medium was prepared with knockout Dulbecco's modified Eagle's medium (DMEM), 20% (vol/vol) KnockOut Serum Replacement, 1% GlutaMax, 1% nonessential amino acids, and 1% penicillin/streptomycin (all from Life Technologies). SNL-CM or MEF-CM was prepared by culturing 3.0×10^6 SNL or 2.4×10^6 MEF feeder cells/10-cm dish with 10 mL of ESC medium supplemented with 4 ng/mL bFGF. Culture medium was collected and replaced with fresh medium every 24 h for 7 d. The collected CM was pooled, filtered, and stored at –20 °C before use.

shRNA Expression Vectors. To construct shRNA expression vectors, we cloned the target sequences into a piggyBac vector that we generated by cloning a U6-driven BsmBI cut site. The original lentiviral construct from which the U6-BsmBI-CNKB region was cloned was kindly provided by Mohammad Mandegar, Gladstone Institutes. shRNAs were designed as two complementary oligonucleotides against targets, containing a polyT 3′ to the shRNA sequence and unique directionally specific sticky ends to the BsmBI cut sites. For each, the two complementary oligos were annealed and ligated into BsmBI-digested piggyBac vector and sequenced for verification.

Silencing the Expression of Genes of Interest. shRNA expression vectors were transfected into Xi-GFP mEpiSCs with Lipofectamine 2000 (Life Technologies). For the transfection, cells were seeded on fibronectin-coated plates with a mixture of DNA (the shRNA expression vector together with piggyBac transposase expression vector) and Lipofectamine mixture in medium containing activin A and bFGF. Twenty-four hours after transfection, the medium was replenished with medium without the DNA-Lipofectamine mixture and changed every 24 h. At 72 h after transfection, 10 μg/mL Blasticidin S (Life Technologies) was added to the medium to select for shRNA-expressing cells. After 4 to 5 d of selection, we started the conversion with the selected cell population. After conversion, the populations that highly expressed mKate fluorescent proteins were sorted (FACS Aria, BD Bioscience) to determine the percentage of GFP^+ cells and to extract RNA for gene expression studies.

RNA Isolation and PCR. Total RNA was purified with TRIzol reagent (Life Technologies) and treated with a Turbo DNA-free kit (Ambion) to remove genomic DNA or with an RNA extraction kit (Qiagen). Total RNA (100 ng to 1 μg) was used for the reverse transcription reaction with SuperScriptIII (Life Technologies) and random hexamer primers, according to the manufacturer's instructions. TaqMan probes and TaqMan Gene Expression Master Mix (Life Technologies) were used to measure gene expression levels.

Western Blotting. To determine phosphorylated and unphosphorylated MLC levels during conversion, Xi-GFP mEpiSCs were cultured in media as indicated in Fig. 4*D* for 6 or 7 d and described in the "Conversion Experiments" section. Then, cells were lysed with RIPA buffer (Sigma) containing phosphatase and protease inhibitors (Sigma; no. 1861280) (300 μL of RIPA buffer per sample) by directly scraping from cell culture plates. After a short incubation on ice, cell debris was removed from the cell lysates by centrifugation (18,700 × *g*, 10 min), and cleared cell lysates were collected in a new tube. To quantify protein concentrations, 1 μL of the cell lysates were diluted with 9 μL of PBS, and protein concentrations were measured with a Nanodrop. We then mixed 300 μL of 2× Laemmli sample buffer (Bio-Rad) with β-mercaptoethanol and 300 μL of cell lysates and then boiled the mixtures at 95 °C for 5 min. Based on the measured protein concentrations, an equal amount of protein from each sample was loaded and separated by electrophoresis on 4–20% (wt/vol) SDS-polyacrylamide gels (456-1094; Bio-Rad) with Tris-SDS running buffer. For the Western blotting for ATX, an equal amount of cell culture supernatants was loaded.

After separation, samples were transferred to a nitrocellulose membrane with the iBlot transfer system (IB3010-01; Invitrogen) with P0 for 5 min. The membrane was blocked with TBS-diluted (1:2 dilution) Odyssey Blocking Buffer (Li-COR Biosciences) for 30 min and then incubated with primary antibodies diluted in the blocking buffer at 4 °C for more than 12 h. After the incubation, the membrane was washed twice with TBS containing 0.1% Tween 20 for 10 min. Then the membrane was incubated with IRDye 680LT (1:20,000)- and/or IRDye 800CW (1:10,000)-conjugated donkey secondary antibody (Li-COR Biosciences) diluted in the blocking buffer supplemented with 0.1% Tween 20. After washing, signals were detected with Odyssey Imaging Systems (Li-COR Biosciences).

Primary antibodies used for Western blotting were rabbit anti-pMLC pS19 (Cell Signaling; 3671; 1:500), mouse anti-MLC (Cell Signaling; 1:500), rabbit anti-GAPDH (Abcam; ab9485, 1:2,000), mouse anti-γTubulin antibody (Abcam; ab11316, 1:5,000), and rabbit anti-ENPP2 (ATX) (Abcam; ab133190, 1:200). Protein expression was quantified by the band intensity with LI-COR imaging software.

Measurement of Autotaxin Enzymatic Activity. Autotaxin enzymatic activities in cell culture media conditioned with Xi-GFP mEpiSCs were measured with the Autotaxin Activity Assay kit (Echelon), according to the manufacturer's instructions. Briefly, the cell culture supernatant (conditioned medium) was gently collected at day 6 or 7 of conversion and centrifuged at 18,700 × *g* for 10 min to remove cell debris. Cleared supernatants were used for the assay. Fluorogenic ATX substrate conjugated with quencher (FS-3) was added

to a reaction mixture. Once ATX cleaves the substrate, the quencher is released from the substrate, and the cleaved substrate increases fluorescent signals. Fluorescent signals were collected with SpectraMax i3x (Molecular Devices) every 2 min for 2 h. The data were analyzed with Microsoft Excel software, which was provided by Molecular Devices, to obtain enzymatic activities (ATX units) for each sample. An ATX units is defined as pM FS-3 hydrolyzed/min in 10 μM FS-3, 50 mM Tris·HCl pH 8.0, 5 mM KCl, 1 mM $CaCl_2$, 1 mM $MgCl_2$, 140 mM NaCl, 1 mg/mL fatty acid-free BSA, and 1 mM lysophosphatidylcholine at 37 °C. Nonconditioned media were used for obtaining background values of the media. Final Autotaxin unit was calculated by subtracting the background values from those obtained with the conditioned media.

Statistical Analysis. All statistical analyses were performed with Microsoft Excel software.

A

	bFGF	ActA	LIF	LPA	AA	BMP-like
mEpiSC medium	12 ng/ml	20 ng/ml	–	No	No	–
SNL-CM	4 ng/ml	< 1 ng/ml	7 ng/ml	Yes	Yes	Yes
MEF-CM	4 ng/ml	13 ng/ml	No	Yes	Yes	Yes

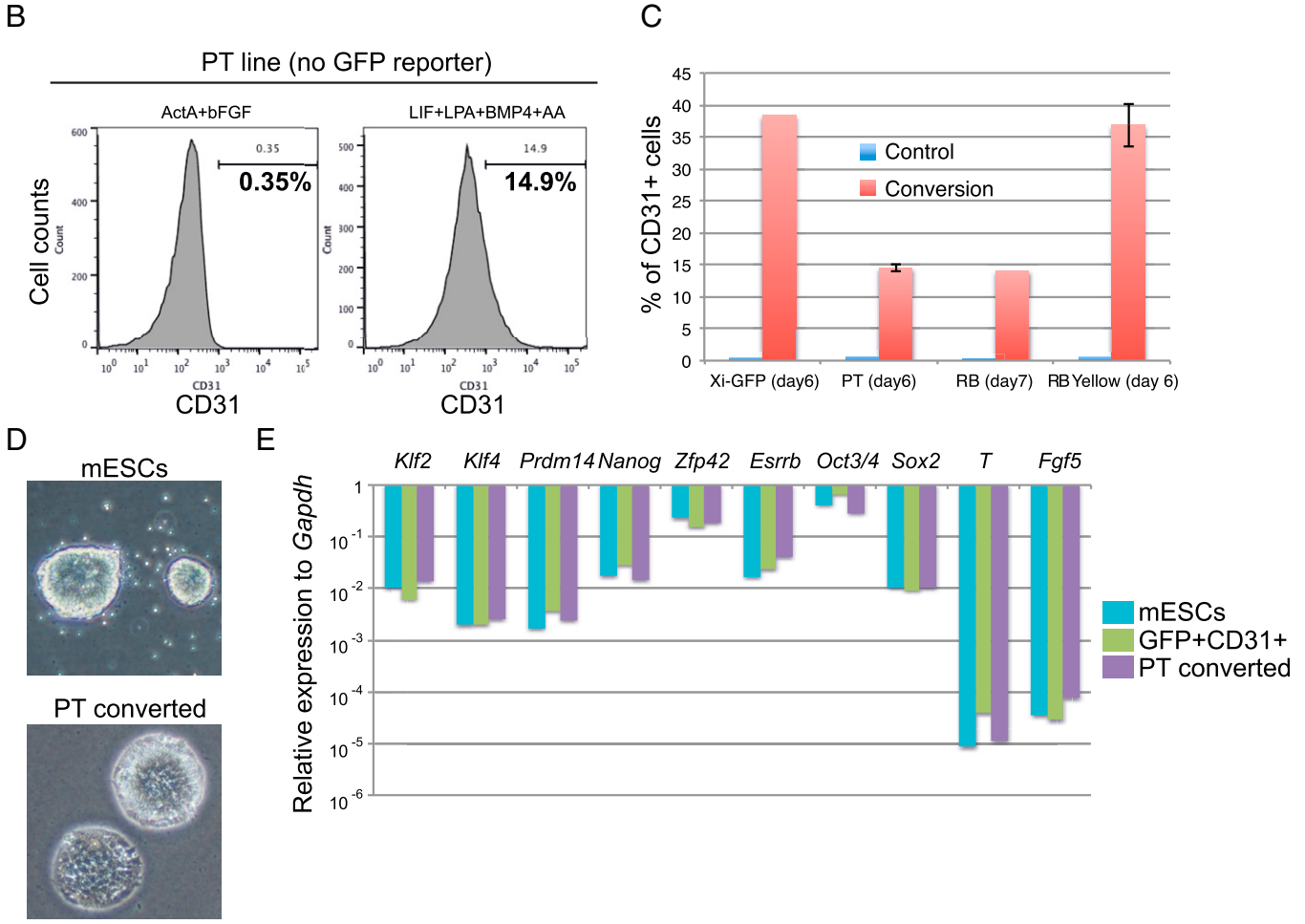

Fig. S1. Conversion medium reproducibly converts mEpiSCs into mESC-like cells. (*A*) Quantification of the concentrations of different factors in the media used. Concentrations of bFGF are the final concentrations of recombinant bFGF added to the media. The concentration of activin A (ActA) in mEpiSC medium is the final concentration of recombinant activin A added. The endogenous concentrations of activin A and LIF in SNL-CM and MEF-CM were determined by ELISA. LPA, AA, and BMP-like activity are from serum replacement. (*B*) FACS histogram showing CD31 (*y* axis) expression in the PT mEpiSC line in mEpiSC medium (ActA+bFGF) or conversion medium (LIF+LPA+BMP4+AA) for 9 d. (*C*) Production of $CD31^+$ cells with four different mEpiSC lines. The percentages of $CD31^+$ cells were determined with the CD31 antibody at day 6 or 7 of conversion in control conditions (blue) or in conversion conditions (red, LIF+LPA+BMP4+AA). The data of Xi-GFP mEpiSCs at day 6 are also used in Fig. 5*B*. Mean ± SD, $n = 1$ for Xi-GFP and RB lines. $n = 2$ for PT and RB Yellow lines. (*D*) Colony morphology of mESCs (E14) and converted PT cells. (*E*) Expression levels, quantified by using qRT-PCR of corresponding RNA, of pluripotency (*Klf2*, *Klf4*, *Prdm14*, *Nanog*, *Zfp42*, *Esrrb*, *Oct3/4*, and *Sox2*) and differentiation (*T* and *Fgf5*) markers relative to *Gapdh* in E14 mESCs (cyan), GFP^+CD31^+ cells (green), and PT converted cells (purple). The bar chart shows mean expression of mRNA levels from one experiment with technical duplicates. PT-converted cells express pluripotency and differentiation markers at similar levels as mESCs and GFP^+CD31^+ cells. The data of mESCs and GFP^+CD31^+ cells are also used in Fig. S2*C*.

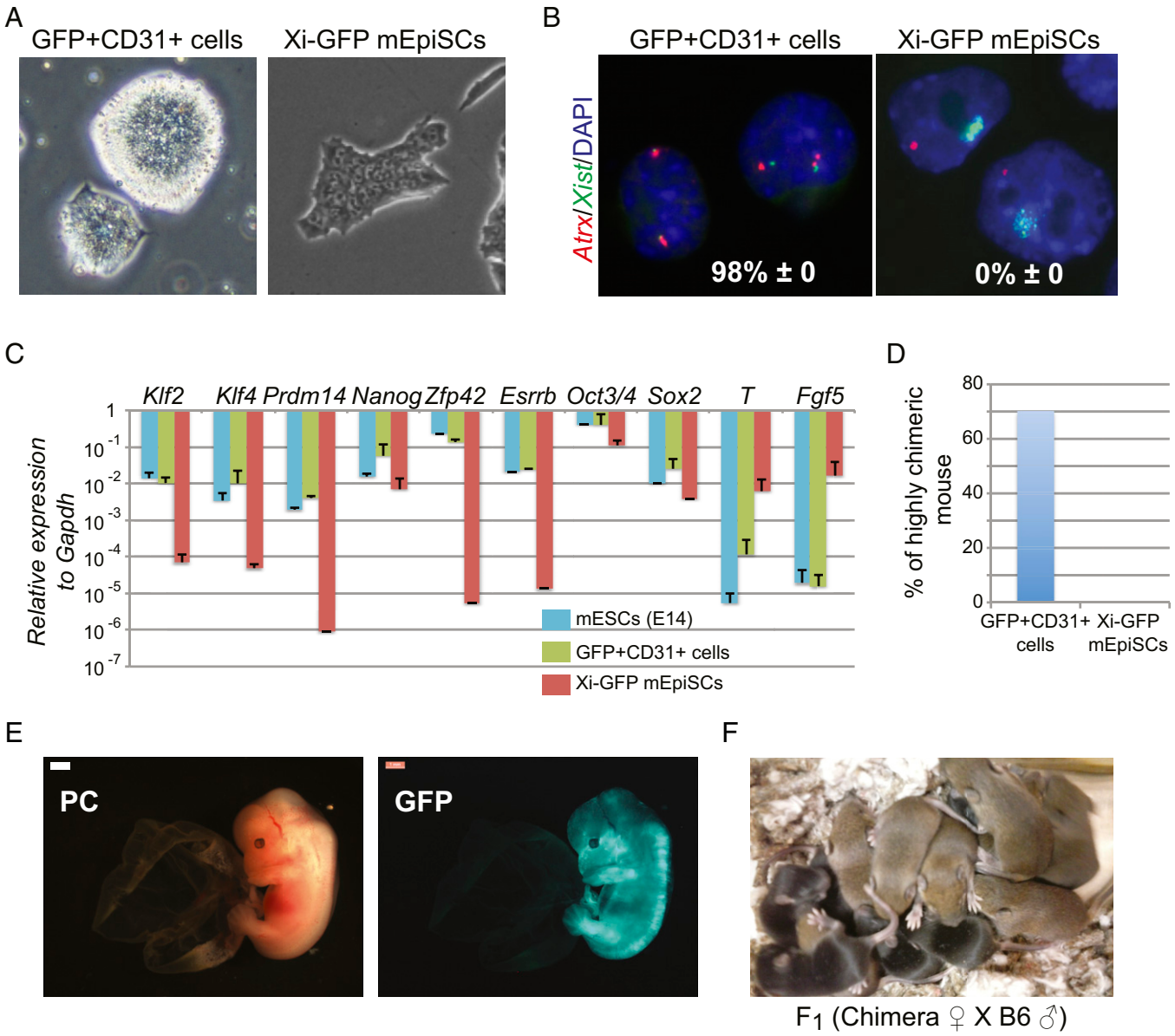

Fig. S2. GFP$^+$CD31$^+$ cells exhibit features of naive pluripotency. (*A*) Picture showing colony morphology of GFP$^+$CD31$^+$ cells and control Xi-GFP mEpiSCs. (*B*) RNA FISH analyses for *Atrx* (red) and *Xist/Tsix* (green) in GFP$^+$CD31$^+$ cells and Xi-GFP mEpiSCs. The percentages of cells that show nascent nuclear foci for both genes are shown as *Inset*. DNA is stained with DAPI (blue). Xi-GFP mEpiSCs show Xist RNA clouds and one site of Atrx nascent transcript accumulation, indicating that they contain one Xi, whereas GFP$^+$CD31$^+$ cells exhibit two sites of nuclear accumulation of *Atrx* and *Xist/Tsix*, indicating that these cells have two Xas. $n = 200$. (*C*) Expression levels of pluripotency (*Klf2*, *Klf4*, *Prdm14*, *Nanog*, *Zfp42*, *Esrrb*, *Oct3/4*, and *Sox2*) and differentiation (*T* and *Fgf5*) markers relative to *Gapdh* in mouse ESCs E14 (blue), GFP$^+$CD31$^+$ cells (green), and parental Xi-GFP mEpiSCs (red). The *x* axis shows the expression levels of the genes, assessed by using RT-quantitative PCR, in logarithmic scale. Mean + SD of biological replicates. $n = 2$ for mESCs, $n = 3$ for GFP$^+$CD31$^+$ cells, and $n = 4$ for Xi-GFP mEpiSCs. (*D*) Percentage of highly chimeric mice obtained after blastocyst injection of GFP$^+$CD31$^+$ cells or parental Xi-GFP mEpiSCs. Ten mice were obtained and analyzed after injection of GFP$^+$CD31$^+$ cells, and 30 mice were obtained and analyzed after injection of parental Xi-GFP mEpiSCs. No chimeric mice were obtained after Xi-GFP mEpiSC injection. (*E*) Images of a chimeric embryo showing contribution of injected GFP$^+$CD31$^+$ cells to mouse development. The GFP-positive embryo shows that GFP$^+$CD31$^+$ cells contribute to mouse development. PC, phase contrast. (Scale bars: 1 mm.) (*F*) Photo of newborn F_1 pups showing germ-line transmission after blastocyst injection of GFP$^+$CD31$^+$ cells. The brown coat color of the pups indicates germ-line transmission.

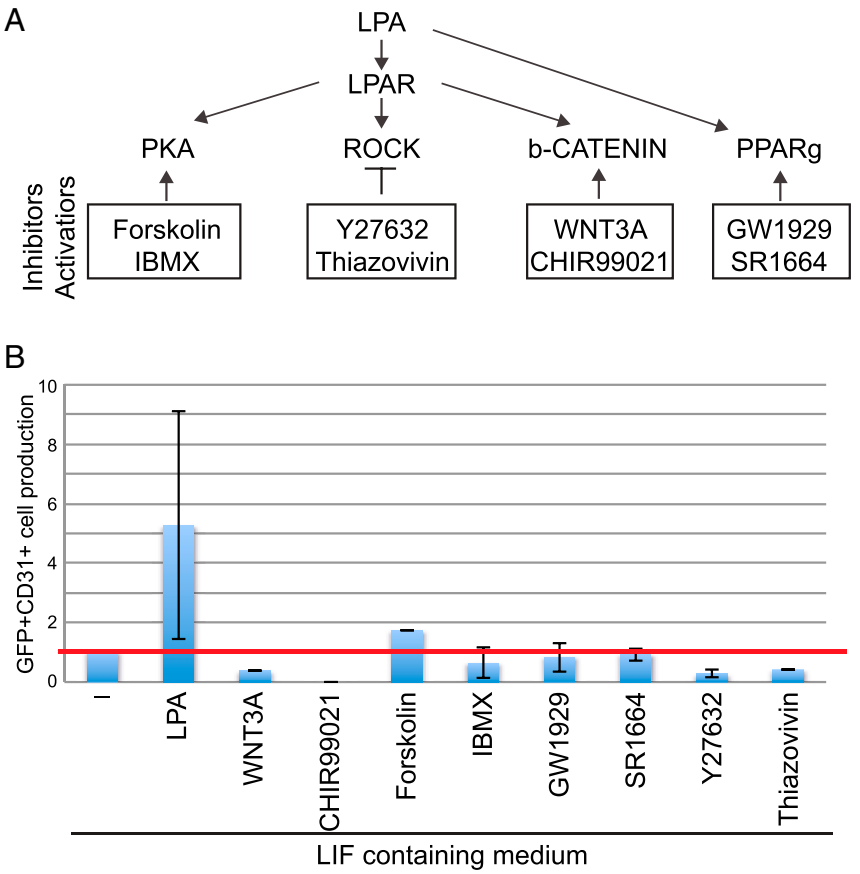

Fig. S3. LPA-LPAR-ROCK signaling promotes GFP$^+$CD31$^+$ cell production. (*A*) Diagram showing LPA signaling pathways, and chemical inhibitors, activators, and modulators of the pathways were analyzed in *B*. (*B*) Relative conversion efficiency of Xi-GFP mEpiSCs, expressed as fold change in percentage of GFP$^+$ CD31$^+$ cells, cultured in various types of media indicated for 13 d. Percentage of GFP$^+$CD31$^+$ cells in N2B27 medium supplemented with LIF alone (–) is set as 1.0. The LIF-containing media were further supplemented with chemical inhibitors, activators, or modulators indicated. Mean ± SD of biological replicates.